Applied Materials Today 18 (2020) 100525

Contents lists available at ScienceDirect

Applied Materials Today

journal homepage: www.elsevier.com/locate/apmt

Hydrophobic to superhydrophilic tuning of multifunctional sporopollenin for microcapsule and bio-composite applications

Ee-Lin Tan [a], Michael G. Potroz [a], Gaia Ferracci [a], Lili Wang [a,b], Joshua A. Jackman [c,*], Nam-Joon Cho [a,*]

[a] School of Materials Science and Engineering, Nanyang Technological University, 639798, Singapore
[b] State Key Laboratory on Integrated Optoelectronics, College of Electronic Science and Engineering, Jilin University, Changchun 130012, China
[c] School of Chemical Engineering, Sungkyunkwan University, Suwon 16419, Republic of Korea

ARTICLE INFO

Article history:
Received 11 November 2019
Accepted 27 November 2019

Keywords:
Biomaterials
Biomimetics
Interfacial science
Colloids
Microencapsulation

ABSTRACT

Sporopollenin sporoderm microcapsules (S-SMCs) are readily extracted from plant pollen grains and provide a renewable, biocompatible source of robust microparticles for a wide range of potential applications. While the lipidic/aromatic sporopollenin copolymer surface results in a predominantly hydrophobic interface, herein, we demonstrate how ultraviolet/ozone (UV-O) light-induced tuning of S-SMC interfacial properties enables production of hydrophobic to superhydrophilic microparticles, along with programmable function for colloidal science and cellular applications. In oil/water systems, stable Pickering emulsions are achieved using S-SMCs with short duration UV-O treatment, while incorporation of superhydrophilic S-SMCs into oil/water systems provides a novel means to produce, and isolate, fully oil-loaded microparticles. Furthermore, it is shown that human cells adhere to S-SMCs acting as tissue seeds, with the controllable formation of either 3D cell spheroids or network structures. Collectively, our findings demonstrate that light-induced modification of S-SMCs has broad implications across colloidal science, microencapsulation, drug delivery, and cellular applications.

© 2019 Elsevier Ltd. All rights reserved.

1. Introduction

There is growing interest in utilizing hollow plant-based sporoderm microparticles, which are extracted from pollen and other sporomorphs, for materials science and biotechnology applications [1–14]. Sporopollenin sporoderm microcapsules (S-SMCs) extracted from pollen have been shown to be highly robust to chemical and physical degradation [15,16], while also showing evidence of biocompatibility and being susceptible to degradation within the human body [17,18]. S-SMCs find broad utility in various applications such as microparticle-stabilized Pickering emulsions, microencapsulation, and drug delivery. In addition to applications that employ native S-SMCs, there are largely untapped opportunities to explore the interfacial properties of the outer sporoderm surface and to develop facile means to modify its surface chemistry to engineer S-SMCs for an expanded range of functional possibilities.

The surface chemistry of S-SMCs is known to be amphiphilic [19] though typically more hydrophobic and therefore light-induced ultraviolet/ozone (UV-O) treatment offers an ideal means to achieve precise control over sporoderm interfacial properties [20,21]. The outer sporoderm layer is comprised of a complex copolymer consisting of a lipidic backbone cross-linked by aromatic compounds [22]. UV-O-induced oxidative processes are known to oxidize both aliphatic [23] and aromatic structures [24] and lead to increased hydrophilicity of such compounds. Additionally, it has been recently shown that defatted pollen particles, including sporopollenin among other components, are susceptible to UV-O treatment and exposure leads to chemical modification and increased wetting properties [25]. However, acid extraction of S-SMCs from pollen capsules is known to alter the polymer structure of the sporopollenin copolymer and hence influence sporopollenin chemical reactivity, the details of which largely remains an outstanding subject [26,27]. Therefore, it remains unknown how acid-extracted S-SMCs will respond to UV-O treatment and whether such modification strategies would be useful for expanding the utility of S-SMCs.

When altering the surface chemistry and interfacial properties of S-SMCs, one of the most important considerations pertains to how the functionalized microparticles can be utilized for colloidal science applications as well as their behavior in more complex biological systems [28,29]. The emulsification potential of acid-extracted S-SMCs as well as native and defatted sporomorphs

* Corresponding author.
E-mail addresses: jjackman@skku.edu (J.A. Jackman), njcho@ntu.edu.sg (N.-J. Cho).

https://doi.org/10.1016/j.apmt.2019.100525
2352-9407/© 2019 Elsevier Ltd. All rights reserved.

has been explored in a handful of studies indicating their potential utility as stabilizing microparticles [19,30]. Additionally, UV-O treatment has been shown to enhance defatted sporomorph dispersion properties and tune Pickering emulsion properties [25]. However, it is currently unclear whether acid-extracted S-SMCs will behave similarly and what are the advantages and limitations of UV-O treatment of S-SMCs for use in aqueous and oil/water systems? Answering such questions can guide targeted development of S-SMCs for colloidal science and microencapsulation applications. One broad microencapsulation area of interest is the loading of hydrophobic compounds into microparticles while ensuring that the consistency of a free-flowing powder remains [31,32]. Until now, attempts to efficiently load oils and hydrophobic compounds into S-SMCs have had limited success, and it has been difficult to obtain a free-flowing oil-loaded powder with high loading efficiencies [17,33,34]. It is proposed that achieving control over the interfacial properties of S-SMCs may allow for enhanced loading potential for hydrophobic compounds, which would significantly expand the overall utility of S-SMCs in a wide range of applications.

Another key area of opportunities lies in interfacing S-SMCs with cellular materials and other biological components. Although S-SMCs are considered a biocompatible material [17,18], there exists very limited information regarding their potential for particle/cell interactions [35,36], and it is unclear how cells may interact with either acid-extracted S-SMCs or UV-O surface modified S-SMCs. Some evidence of cell adhesion to defatted natural pollen particles has been reported, with UV-O surface modification enhancing pollen/cell binding [25]. Extending these capabilities to the more versatile hollow core/shell microparticle structure of S-SMCs might further enable a range of particle/cell systems with broad application possibilities [37–40].

Inspired by these possibilities, the goal of this study is to explore how S-SMCs generated from *Camellia sinensis* bee-collected pollen can be modified by UV-O treatment and thereby utilized in oil/water based systems, for enhancing oil loading, and to further understand how mammalian cells interact with untreated and UV-O treated S-SMCs serving as tissue seeds (Fig. 1). To this end, hollow S-SMCs were extracted from defatted *C. sinensis* pollen and extensively characterized with respect to surface morphology and other fundamental properties. The effect of UV-O treatment was observed with regards to particle morphology and wetting properties. Particle surface chemistry was explored before and after UV-O treatment *via* x-ray photoelectron spectroscopy (XPS) and Fourier-transform infrared spectroscopy (FTIR) analysis to gain insight into the fundamental chemical mechanisms driving alterations in interfacial properties. Emulsification properties were explored to elucidate the potential for S-SMCs to form Pickering emulsions and determine the limitations of UV-O treatment on tuning emulsion properties. Insights gained from studying emulsion dynamics were used to explore and optimize S-SMC oil loading potential. Finally, particle/cell binding dynamics were explored with untreated and UV-O treated S-SMCs and Huh-7.5 liver hepatocarcinoma cells to determine whether cells can adhere to S-SMCs, and how fundamental aqueous suspension properties influence particle/cell interactions with a long view towards achieving hierarchical control over formation of tissue-like architectures.

2. Material and methods

2.1. Materials

Bee-collected pollen pellets from *Camellia sinensis* were procured from Xi'an Yuensun Biological Technology Company Limited (China). Acetone was purchased from Aik Moh Paints & Chemicals Pte Ltd (Singapore). Diethyl ether, absolute ethanol, and hydrochloric acid were purchased from Merck Millipore Corporation (USA). Phosphoric acid, sodium hydroxide, isopropyl myristate, sodium chloride, acetanilide standards, and Nile red were obtained from Sigma-Aldrich Pte Ltd (USA). Nylon mesh was procured from ELKO Filtering Co. LLC (USA). Tin weighing boats were obtained from Elementar Vario EL III (Germany). Duke polystyrene microsphere standards (50 ± 1 μm) were procured from Thermo Scientific Pte Ltd (USA). Cocoa butter was purchased from Phoon Huat Pte Ltd (Singapore).

2.2. Defatting of bee pollen granules

Defatting was performed using acetone, water, and diethyl ether. *C. sinensis* bee pollen pellets (250 g) were refluxed in acetone (500 ml, 50 °C, 220 rpm, 3 h). Acetone was removed and the sample was bath-sonicated (10 min) with deionized (DI) water (1000 ml, 50 °C). The pollen solution was passed through nylon mesh (150 μm), followed by mixing with DI water (1000 ml, 50 °C) and then vacuum filtration. The resulting sample was refluxed in acetone (500 ml, 50 °C, 220 rpm, 3 h). Acetone was removed and the sample was left to dry in a fume hood. Dry sample (20 g) was mixed with diethyl ether (250 ml, 25 °C, 300 rpm, 2 h, 2 times). The sample was stirred in diethyl ether (250 ml, 25 °C, 300 rpm, 12 h). The sample was transferred to a petri dish and left to dry in a fume hood after diethyl ether was removed.

2.3. Extraction of S-SMCs

Defatted *C. sinensis* pollen particles (60 g) were refluxed (70 °C, 220 rpm, 1 h, 3 h, 5 h and 10 h) with phosphoric acid (85 % (w v^{-1}), 600 ml) in a round bottom flask. Phosphoric acid was removed with the aid of vacuum filtration and extracted S-SMCs were washed with DI water (500 ml, 50 °C, 5 times), acetone (500 ml, 50 °C, 2 times), sodium hydroxide solution (2 M, 500 ml, 50 °C), hydrochloric acid solution (2 M, 500 ml, 50 °C), DI water (500 ml, 50 °C, 5 times), acetone (500 ml, 50 °C), ethanol (500 ml, 50 °C, 2 times), and DI water (500 ml, 50 °C). Washing was done with stirring using a spatula.

2.4. CHN elemental analysis of S-SMCs

Acid extracted S-SMCs were dried (5 mg) and analyzed by CHN elemental analysis (Elementar Vario EL III, Germany) to ascertain removal of nitrogen and estimate protein removal. Acetanilide (5 mg) was analyzed to calibrate the machine before the sample run.

2.5. Ultraviolet-Ozone (UV-O) treatment

UV-O treatment was carried out on S-SMCs (50 mg) for various durations (1, 5, 15, or 30 min). S-SMCs were spread evenly on a plastic disposable petri dish (90 mm x 15 mm) and exposed to UV-O (12188 W m^{-1}) using a benchtop PSD Series UV-O cleaner (Novascan, USA).

2.6. Contact angle measurements

Contact angle measurements were performed with S-SMCs (0, 1, 5, 15, or 30 min UV-O treated). A thin layer of pollen was spread on self-adhesive carbon tape (5 mm x 5 mm) on a glass slide and a bead of DI water (2 μl) was slowly lowered onto the layer of S-SMCs. The contact angle was measured using an Attension Theta Optical Tensiometer (Biolin Scientific Holding AB, Sweden) (0.7 X magnification, 20 s, 12 FPS) with OneAttension 1.0 software.

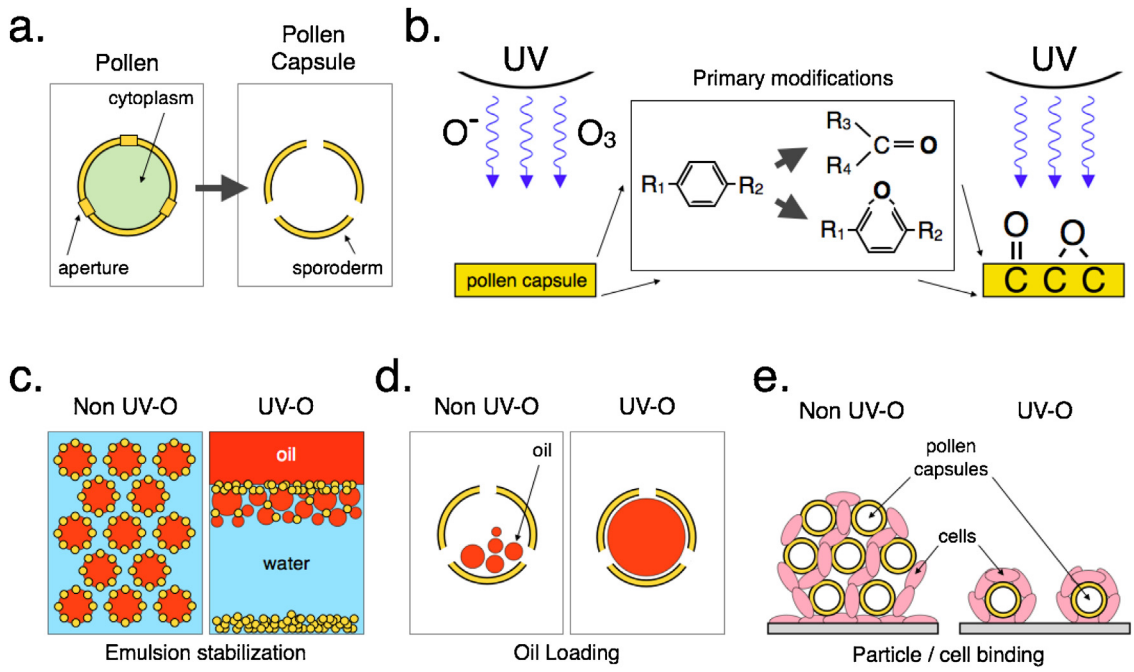

Fig. 1. Sporopollenin sporoderm microcapsule (S-SMC) extraction and ultraviolet-ozone (UV-O) surface modification allow for tunable microparticle emulsification, oil loading, and particle/cell binding. (a) Acid extraction of S-SMCs from pollen. (b) UV-O treatment of pollen capsules with primary chemical modifications. (c) Emulsion stabilization before and after extensive UV-O treatment. (d) Oil loading before and after UV-O treatment. (e) Particle/cell binding before and after UV-O treatment.

2.7. X-ray photoelectron spectroscopy

Wide (160 eV) and narrow (20 eV) scan XPS was performed with pollen particles (0 or 30 min UV-O treated). S-SMCs were dried using a freeze drier overnight before UV-O treatment. S-SMCs were deposited on carbon tape (5 mm x 5 mm) adhered to a silicon wafer. Samples were analyzed using AXIS Supra (XPS) surface analysis instrument (Kratos Analytical Ltd, United Kingdom) equipped with a monochromatic Al/Mg X-ray source (225 W, 2×10^{-9} mbar). Spectra were obtained using an aluminum anode (Al Kα =1491.600 eV) and charge neutralization.

2.8. Attenuated total reflection Fourier-transform infrared spectroscopy

ATR-FTIR was performed using Perkin Elmer Frontier FT-IR spectrometer with a universal ATR sampling accessory (Perkin Elmer Inc, USA). Absorbance spectra of S-SMCs (0, 1, 5, 15, or 30 min UV-O treated) were collected. Samples were scanned, backgrounded, baselined, and smoothed using Spectrum v10.5 program. Six separate sets of ATR-FTIR spectra were collected for each sample and were normalized to a standard peak (1063 cm^{-1}). Peak heights of specific functional groups were extracted and ratios between functional group peak heights were calculated.

2.9. Dynamic image particle analysis

Dynamic image particle analysis was performed using bench top FlowCAM® (Fluid Imaging Technologies Inc., USA). The system was setup with a lens (4x), a flow cell (200 μm) at a constant flow rate (0.25 ml min^{-1}). For particle/cell adhesion quantification, aqueous solution of extracted S-SMCs (1 ml) was prepared and analyzed to determine solution concentration and quantify particles.

2.10. Pickering emulsions

Pickering emulsions were made using S-SMCs (0, 1, and 30 min UV-O). Suspensions of S-SMCs (100 mg) in isopropyl myristate (5 ml) were made with the aid of a probe sonicator (probe tip diameter of 30 mm, 20 kHz, 10 W, 2 min), then added to a glass vial (20 ml) containing sodium chloride solution (10 mM, 5 ml). Water phase, oil phase, and particle system was then vortexed (speed 10, 5 min). For imaging purposes to differentiate between oil and water, the oil phase was dyed with Nile red (0.3 mg ml^{-1}). Heights of the emulsion, oil, and water layer were recorded initially and after one week.

2.11. Cocoa butter oil loading

C. sinensis S-SMCs (250 mg) were added to cocoa butter (5 ml, 40 °C), vortexed (speed 10, 1 min), and then transferred to a vial containing DI water (5 ml, 40 °C) and homogenized using a IKA Ultra Turrax T18 rotorstator mixer (IKA Works GmbH & Co. KG, Germany) (1.0 cm dispersing head, 19 000 rpm, 2 min). Resulting emulsion (1 ml) was transferred using a disposable dropper to a separating funnel (100 ml) and left to stand in the fridge (10 °C, 30 min) for cocoa butter to harden. Hot water (50 ml, 90 °C) was added to the separating funnel and left to stand (25 °C, 12 h) for S-SMCs to settle. Sedimented S-SMCs were collected and analyzed. A second extraction was performed for collection and isolation of floating S-SMCs.

2.12. S-SMC/Cell adhesion study

Sterilized S-SMC particles in media were incubated with human hepatocyte carcinoma cells. Cells (160,000 cells per well) were seeded in 24-well tissue culture plate (37 °C, 5 % CO_2, 24 h) with culture media (1 ml) made of Dulbecco's Modified Eagle Medium (1x), fetal bovine serum (10 %), and penicillin-streptomycin (1 %).

Culture media was removed and S-SMC particles (40 000) were added to each well (1 ml, 0.16 mg ml^{-1}) and incubated (37 °C, 5 % CO_2, 24 h). Culture media was collected from wells and samples were washed with culture media (1 ml, 3 times). Unbound S-SMC particles were collected from supernatants by centrifugation (5000 × *g*, 25 °C, 5 min). Quantification of unbound S-SMC particles were done using DIPA.

2.13. CLSM analysis

CLSM was performed using a Zeiss 710 Confocal Microscope (Carl Zeiss AG, Germany). Calcein acetoxymethyl in culture media (1 μL ml^{-1}) was added to samples for cell studies and incubated (1 h, 37 °C, 5 % CO_2) and imaged in a 24-well culture plate. Imaging of Pickering emulsions was done by transferring some of the emulsion onto a glass slide. Imaging was performed successively with three laser excitation channels: 405, 488, and 561 nm, with three respective emission filters: 416–477, 498–550, and 572–620 nm and objective lens (20×). At least three images were captured per sample. Z-stack slices were taken (Z-stack thickness of 4 μm, 5 μm interval, bidirectional laser scanning, scan speed of 6, pixel averaging of 2, 12 slices). For particle/cell distribution analysis, images were processed using ImageJ by converting to 8 bit and thresholding to define solid regions of particles or cells, followed by quantifying the proportion of regions of interest.

2.14. Bright field microscopy

Bright field microscopy was performed using a Nikon Eclipse Ti-E Inverted Microscope System (Nikon Instruments Inc., USA) with NIS-Elements AR Microscope Imaging Software Version 4.0 (Nikon Instruments Inc., USA). Videos of S-SMCs and cells in a 24-well culture plate being agitated with a micropipette were recorded (5 FPS for 1 min) (Supplementary information, Video S1).

2.15. Surface morphology evaluation by scanning electron microscopy

SEM imaging was performed using an FESEM JSM 7600 F (JEOL, Japan). Briefly, gold coating (20 mA, 80 s, distance from target is 3 cm) was applied with an auto fine coater JFC-1600 (JEOL, Japan) and images were taken (acceleration voltage of 5.00 kV at various magnifications). Fixing of cells was done with glutaraldehyde solution (4 %, 1 ml, 40 min), washed with PBS (1 ml, 5 min, 3 times) and dehydrated with ethanol sequentially (1 ml, EtOH 25 %, 50 %, 75 %, 95 %, 100 % for 20 min each). After fixing, samples were frozen (−80 °C, 12 h) and lyophilized (24 h).

2.16. Evaluation of Pickering emulsion by stereomicroscopy

Stereomicroscope imaging was performed with a Nikon SMZ1000 Zoom Stereomicroscope (Nikon Instruments Inc., USA) with an LV-TV adapter connected to a digital camera and NIS-Elements F Microscope Imaging Software Version 4.0 (Nikon Instruments Inc., USA). The emulsion was transferred from the glass vial onto a glass slide and images were taken at several magnifications.

2.17. Statistical analysis

Quantitative data were collected in triplicate and were expressed as mean and standard deviation (SD). Two-tailed t-tests, with $P < 0.05$ being statistically significant were performed for statistical analysis of data.

3. Results and discussion

3.1. Microcapsules may be extracted from bee pollen granules

Pollen microcapsules, S-SMCs, were extracted from bee-collected pollen by a two-step process including isolation of discrete pollen particles from bee pollen granules, followed by acid extraction of hollow S-SMCs from the discrete pollen particles. Optimization of S-SMC acid-extraction was conducted for varying acidolysis durations to determine the minimum extraction time required to achieve adequate removal of cytoplasmic contents. Elemental analysis of percent nitrogen (N%) is commonly used to identify the proportion of proteinaceous material present during S-SMC extraction, and N% multiplied by a factor of 6.25 is used to estimate percent protein [41]. Defatted pollen, and acidolysis durations of 1, 3, 5, and 10 h, resulted in protein contents of 61.5 ± 0.3 %, 11.7 ± 0.1 %, 3.9 ± 0.0 %, 3.4 ± 0.3 %, and 3.0 ± 0.0 %, respectively (Supplementary Information, Fig. S1). The data indicates that 3 h treatment provides maximum protein removal based on standard acidolysis extraction methods. Numerous studies with other pollen species have indicated similar levels of proteinaceous residues even with longer duration high-temperature acidolysis [41,42]. It has been shown by matrix-assisted laser desorption/ionization time-of-flight mass spectrometry (MALDI-TOF MS) that all proteinaceous materials above 1 kDa are effectively removed by similar S-SMC acid extraction [43,44]. Low levels of nitrogen content commonly observed during acid extraction may be attributed to residual amino acids adhered to the S-SMC.

Micromeritic analysis of defatted pollen and S-SMCs extracted with acidolysis durations of 1, 3, 5, and 10 h, resulted in particle diameters of 36.6 ± 0.1, 33.8 ± 0.4, 32.8 ± 0.3, 31.3 ± 0.3, and 32.2 ± 0.1 μm, respectively, and minimal variation in morphological parameters such as circularity and aspect ratio (Supplementary Information, Fig. S2). Scanning electron microscopy (SEM) and confocal laser scanning microscopy (CLSM) analysis of defatted pollen and S-SMCs extracted with acidolysis durations of 1, 3, 5, and 10 h, indicated that all acidolysis durations appeared to remove cytoplasmic contents and produced hollow S-SMCs (Fig. 2 and Supplementary information, Fig. S3). Therefore, based on the results of elemental analysis, micromeritic analysis, and microscopy analysis, it was decided to use 3 h acid extracted S-SMCs for the remainder of the study. Of note, S-SMC extraction yields from defatted pollen were 17.3 ± 2.1 %, comprising 245,075 ± 33,032 particles mg^{-1} with a particle weight of 4.1 ± 0.5 ng. Considering a sporoderm wall thickness of 1.2 ± 0.1 μm, the sporoderm density is 1.09 ± 0.20 g cm^{-3}, which is consistent with the observation that S-SMCs sink in water.

3.2. UV-O exposure alters pollen microcapsule surface chemistry

UV-O treatment of S-SMCs with UV-O treatment durations of 0, 1, 5, 15, and 30 min, resulted in no changes in overall particle morphology and no distinct changes in nano-scale surface morphology (Fig. 2b,c and Supplementary Information, Fig. S4). Significant increases in wetting were observed within 1 min of UV-O treatment with the particles becoming superhydrophilic within 15 min. Contact angle measurements of S-SMCs with UV-O treatment durations of 0, 1, 5, 15, and 30 min resulted in contact angles of 100.2 ± 12.6°, 34.9 ± 13.1°, 14.2 ± 2.6°, 7.2 ± 0.6°, and 5.9 ± 2.0° (Fig. 2d), respectively. Overall, these observations suggest that enhanced particle wetting may be attributed to variations in the surface chemistry of the S-SMCs.

UV-O induced surface chemistry changes are predominantly driven by increases in total oxygen content, with increased proportions of ketone ($R_2C=O$) binding and carbon-oxygen (COR) binding. Wide-scan XPS analysis indicates that total atomic oxygen

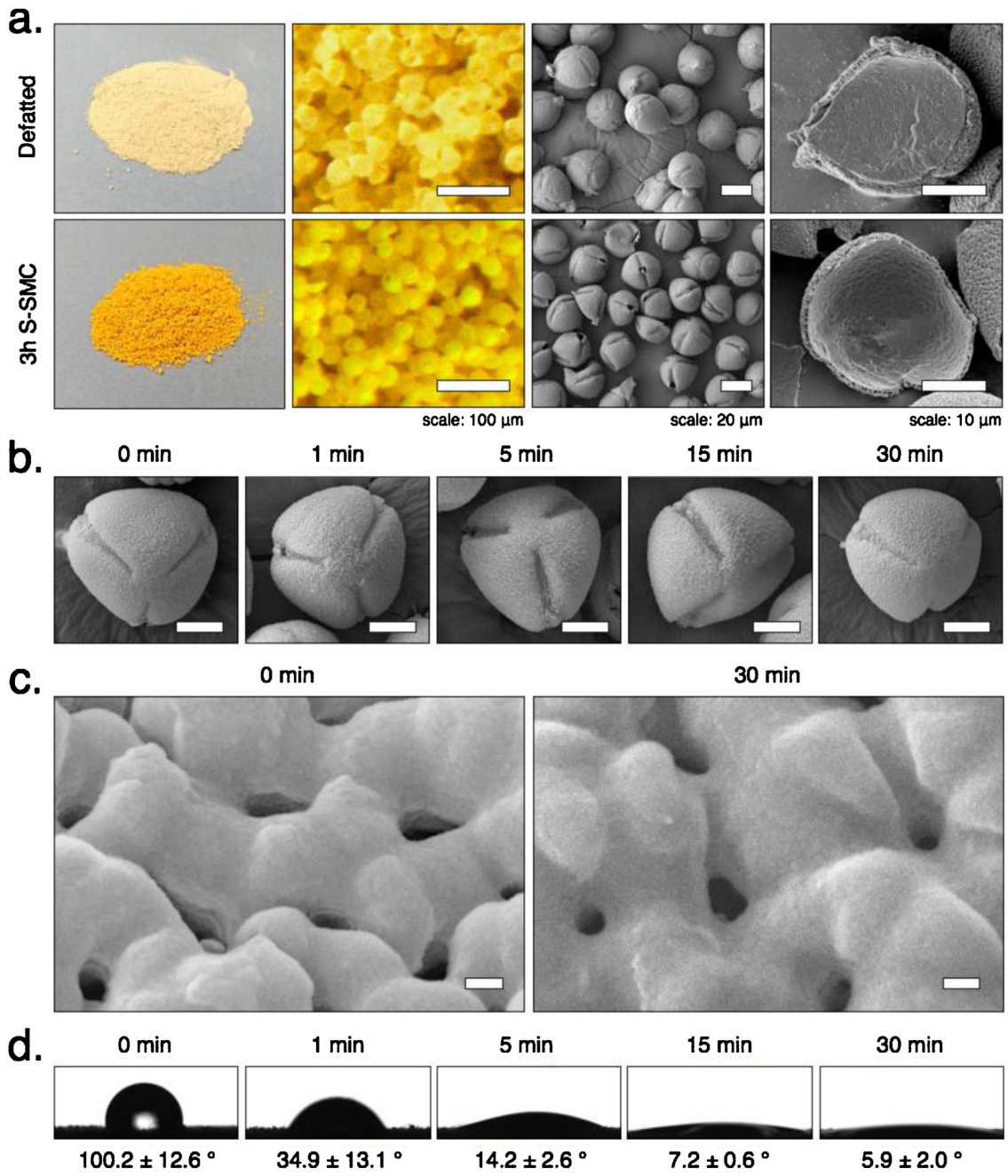

Fig. 2. Sporopollenin sporoderm microcapsule (S-SMC) extraction and ultraviolet-ozone (UV-O) surface modification effects on particle morphology and wetting properties. (a) Photographs, optical stereomicrographs, and scanning electron microscopy (SEM) images of defatted *C. sinensis* pollen and 3 h acid-extracted hollow S-SMCs. (b) SEM images of overall particle morphology with UV-O treatment from 0–30 min. Scale bars, 10 µm. (c) SEM images of particle surface morphology with an untreated and 30 min UV-O treated S-SMC. Scale bars, 100 µm. (d) Optical microscope images of water droplets during contact angle measurements of S-SMCs with UV-O treatment from 0–30 min.

Table 1
Bond-type binding energies and proportions for carbon (C1s) and oxygen (O1s) binding.

	Carbon (C1s)					Oxygen (O1s)			
#	Bond type	Binding energy [eV]	0 min [%]	30 min [%]	#	Bond type	Binding energy [eV]	0 min [%]	30 min [%]
6	CC / CH	284.8	35.6 ± 4.7	30.7 ± 1.4					
5	COH	285.7	20.5 ± 0.8	17.5 ± 0.5	10	COH	532.7	23.8 ± 1.8	21.4 ± 1.1
4	COC	286.8	13.7 ± 1.8	22.6 ± 1.7	9	COC	533.0	12.3 ± 1.4	20.2 ± 1.8
3	$R_2C{=}O$	287.8	15.7 ± 2.4	19.7 ± 3.4	11	$R_2C{=}O$	531.6	12.9 ± 3.1	18.8 ± 1.6
2	RO-C=O	288.8	11.7 ± 2.4	6.5 ± 1.1	8	CO-C=O	534.1	33.7 ± 0.6	25.2 ± 0.4
					7	HO-C=O	535.5	17.3 ± 1.4	14.5 ± 1.7
1b	π-π	291.0		3.1 ± 0.9					
1a	π-π	291.7	2.8 ± 0.8						

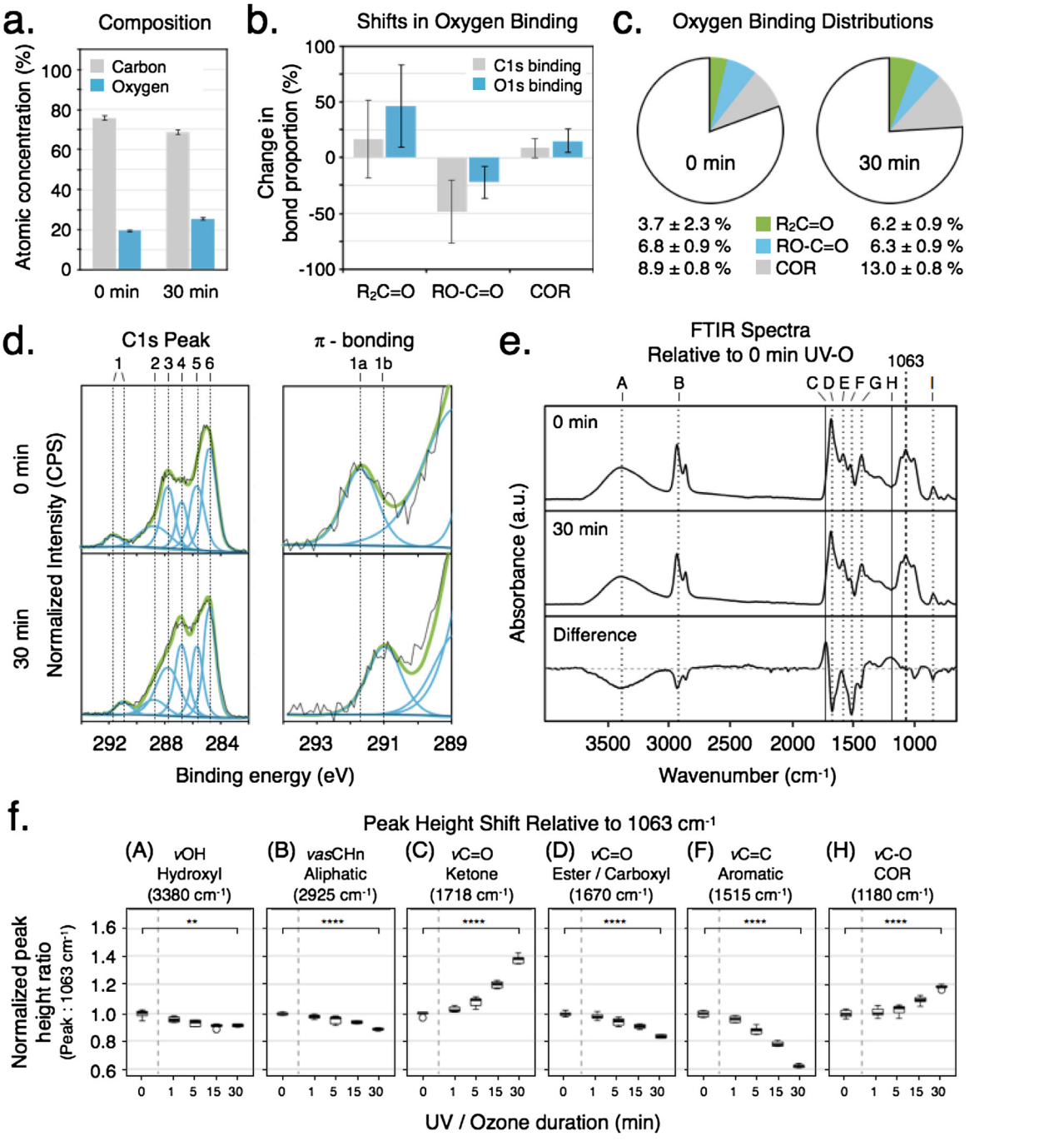

Fig. 3. Surface chemistry analysis of untreated and ultraviolet-ozone (UV-O) **treated sporopollenin sporoderm microcapsules (S-SMCs).** (a) XPS quantification of atomic carbon and oxygen. (b) XPS quantification of proportional shifts in major oxygen binding groups. (c) XPS quantification of overall oxygen binding distributions. (d) XPS narrow scan carbon (C1s) peak of untreated and UV-O treated S-SMCs. (e) ATR-FTIR spectra and difference analysis of untreated and UV-O treated S-SMCs. (f) Normalized peak height ratio analysis of key peaks of interest from ATR-FTIR spectra.

increases and total atomic carbon decreases with UV-O treatment durations of 0 and 30 min resulting in oxygen concentrations of 19.4 ± 0.6 % and 25.5 ± 0.9 %, and carbon concentrations of 75.8 ± 1.3 % and 68.6 ± 1.4 %, respectively (Fig. 3a and Supplementary Information, Fig. S5a). With regards to oxygen binding distributions, narrow scan XPS analysis of both C1s and O1s peaks indicates that $R_2C{=}O$ binding increases by ~31 %, carboxylic acid/ester (RO-C=O) binding decreases by ~35 %, and COR binding increases by ~12 % with 30 min UV-O (Fig. 3b and Supplementary Information, Fig. S5b). Combining both total atomic oxygen and binding distribution data, it is possible to quantify overall oxygen binding distributions before and after UV-O treatment. With 30 min UV-O treatment the total proportion of $R_2C{=}O$ nearly doubles from 3.7 ± 0.5%–6.2 ± 0.8 %, the total proportion of RO-C=O decreases slightly from 6.8 ± 0.6%–6.3 ± 0.6 %, and the total proportion of COR increases by half from 8.9 ± 0.3%–13.0 ± 0.5 % (Fig. 3c). It is important to note that upon more detailed analysis of the narrow scan XPS data, the increase in COR binding can be attributed to ether (COC) binding rather than COH binding (Table 1).

UV-O treatment of S-SMCs influences π-bonding, suggesting that one mechanism of acid-extracted sporopollenin oxidation involves alterations of aromatic ring structures without causing

complete ring opening. It is unknown how acid extraction of S-SMCs alters sporopollenin chemistry. However, comparing the narrow scan carbon (C1s) peak structure from S-SMCs in this study with (C1s) peak structure data from a previous study of defatted-only *C. sinensis* sporopollenin [25], acid-extraction is shown to introduce a small peak at 291.7 eV (Fig. 3d and Supplementary Information, Fig. S5b), which may be attributed to π-bonding from aromatic ring stacking [45]. Of note, this is the first observation of aromatic ring stacking in sporopollenin due to acid-extraction, and has important implications for material property analysis of sporopollenin, including for palynological studies of pollen fossils used in climate change analysis [46]. Further, upon S-SMC exposure to UV-O, there is a clearly defined shift in the π-bonding peak energy from 291.7 eV to 291.0 eV, which suggests an alteration of aromatic ring structure without causing complete ring opening. Based on oxidation of carbon rings in graphene [47,48], it is proposed that π-bonded rings in sporopollenin undergo a process of epoxidation leading to the insertion of atomic oxygen to replace CC bonds and form COC ether bonds, which is supported by the increase in COC bonds observed from both C1s peak and O1s peak analysis with UV-O treatment (Table 1).

ATR-FTIR analysis of UV-O treated S-SMCs supports the conclusions from XPS analysis and provides deeper insights into the overall trends in surface chemistry. FTIR spectra showed no major appearances or disappearances of peaks with UV-O treatment (Fig. 3e and Supplementary Information, Fig. S6a). However, a difference analysis of S-SMC FTIR spectra before and after UV-O treatment revealed that most prominent peaks observable in the raw FTIR spectra show successive reductions in peak height with increasing UV-O treatment duration (Fig. 3e and Supplementary Information, Fig. S6b). Additionally, with difference analysis, two regions become highlighted and show prominent increases, 1718 cm^{--1} and 1180 cm^{-1}. Peak height ratio analysis was used to quantify the trends observed from the difference analysis by comparing the height of each peak of interest to the height of the stable major peak at 1063 cm^{-1}. Previous studies regarding pollen have attributed peaks around 1063 cm^{-1} to COR bonds of cellulosic compounds present in the cellulosic inner sporoderm layer [49]. It is expected that the intine layer will be protected from UV-O treatment by the outer sporoderm layer and will provide a stable reference peak for use in peak height ratio analysis. Other FTIR peaks used for peak height ratio analysis are assigned based on existing literature as follows [50–52], A: hydroxyl (*ν*OH, 3380 cm^{-1}), B: aliphatic (*vas*CH_n, 2925 cm^{-1}), C: ketone (*ν*C═O, 1718 cm^{-1}), D: carboxylic acid/ester (*ν*C═O, 1670 cm^{-1}), E: aromatic (*ν*C═C, 1575 cm^{-1}), F: aromatic (*ν*C═C, 1515 cm^{-1}), G: aromatic (*δ*C-H, 1425 cm^{-1}), H: ether (*ν*C—O, 1180 cm^{-1}), and I: aromatic (*δ*C-H, 840 cm^{-1}).

Peak height ratio analysis indicates that the major changes in polymer chemistry are increases in ketone (R_2C═O) binding and ether (COC) binding, with the largest proportional decreases in aromatic ring (C═C) binding (Fig. 3f and Supplementary Information, Fig. S7). The relative peak height ratios of all peaks of interest, after 30 min UV-O treatment, are A = 0.92 ± 0.01, B = 0.89 ± 0.01, C = 1.39 ± 0.03, D = 0.84 ± 0.01, E = 0.94 ± 0.1, F = 0.63 ± 0.1, G = 0.86 ± 0.01, H = 1.19 ± 0.01, and I = 0.73 ± 0.3. The trends of increasing ketone (R_2C═O) binding and ether (COC) binding are consistent with the binding trends observed with XPS. Decreases in aromatic ring (C═C) binding may be attributed to UV-O induced aromatic ring opening [25]. Importantly, the oxidative degradation of the aromatic compound *p*-coumaric acid has been shown to produce ketone (R_2C═O) moieties [24], and *p*-coumaric acid is known to be one of the major constituents of sporopollenin [22]. Therefore, the increase in ketone (R_2C═O) bonds may be directly attributable to UV-O induced aromatic ring opening within sporopollenin.

Overall, both XPS and FTIR analysis suggest that aromatic rings in acid-extracted sporopollenin present two possible paths of oxidation. Firstly, some aromatic rings may be cleaved open during UV-O exposure leading to the formation of ketone bonds (R_2C═O), and secondly, some π-bonded aromatic rings undergo alteration of the ring structure with the formation of ether bonds (COC). It should be noted that oxidation of the aliphatic chains present in the copolymer structure may contribute to ketone bond (R_2C═O) formation [23], although UV-O oxidation studies with aliphatic polymers such as polyethylene indicate increases in atomic oxygen of less than 1 % after complete oxidation [53], which is much less than the ~6 % atomic oxygen increase observed above.

3.3. UV-O exposure alters Pickering emulsion properties

UV-O treatment of S-SMCs alters emulsion properties when S-SMCs are used for forming microparticle stabilized Pickering emulsions (Fig. 4). Untreated S-SMCs or UV-O treatment for short duration facilitated the formation of microparticle stabilized Pickering emulsions, however, long duration UV-O treatment resulted in lower quality emulsions. Emulsions were prepared using equal parts oil and water with the addition of 0, 1, or 30 min UV-O treated S-SMCs and stabilized for 7 days. Emulsions formed with 0, 1, and 30 min treated S-SMCs resulted in systems with oil fractions (f_{oil}) of 0.65 ± 0.03, 0.80 ± 0.01, and 0.83 ± 0.03, and aqueous fractions (f_{aq}) of 0.70 ± 0.03, 0.80 ± 0.06, and 0.74 ± 0.03, respectively (Fig. 4a).

Emulsions formed with untreated S-SMCs appear well-structured with a relatively uniform droplet size with the majority of droplets ranging from 250−500 μm, however, utilizing UV-O treated S-SMCs produces greater droplet size variability with an overall reduction of average droplet sizes, with the majority of droplets ranging from 50−250 μm, and some settling of particles (Fig. 4b). Observing the bottom of the emulsion layer *via* CLSM shows that for untreated particles there are relatively few discrete settled particles and most S-SMCs observed are in the proximity of an oil droplet, stained red with a hydrophobic dye (Nile Red) (Fig. 4c and Supplementary Information, Fig. S8). Incorporating 1 min UV-O treated S-SMCs results in many more settled particles and small oil droplets, suggesting a limited degree of S-SMC/oil interaction. Incorporating 30 min UV-O treated S-SMCs results in only settled particles with no oil drops visible, suggesting little S-SMC/oil interaction. Observations of emulsion structures from above with standard optical stereomicroscopy further indicates that untreated S-SMCs produce emulsions wherein the particles surround and attach to oil droplets, with 1 min U-VO resulting in some particle/oil affinity, and 30 min UV-O resulting in minimal particle/oil affinity leading to less stable and less ideal emulsions (Fig. 4d and Supplementary Information, Fig. S9). It has been observed in previous studies that UV-O treatment durations of up to 120 min may be applied to hydrophobic defatted pollen particles to tune Pickering emulsion properties [25]. However, the contact angles of UV-O treated pollen plateaued at ~55°, whereas, the contact angle of S-SMCs with 1 min UV-O has already reduced to ~35°. Therefore, to utilize UV-O for tuning S-SMC stabilized Pickering emulsions, it may be necessary to limit the UV-O treatment duration to less than 1 min.

3.4. UV-O exposure facilitates optimal microcapsule oil-loading

Standard emulsion preparation techniques in conjunction with UV-O treated S-SMCs provide a facile means for loading oil within S-SMCs and enables the isolation of only fully loaded S-SMCs. The above-mentioned investigations into utilizing S-SMCs in Pickering emulsions resulted in the observation that emulsion homogenization could be used to load tiny oil droplets into the hollow S-SMC internal cavity through the micron-sized apertures in the shell

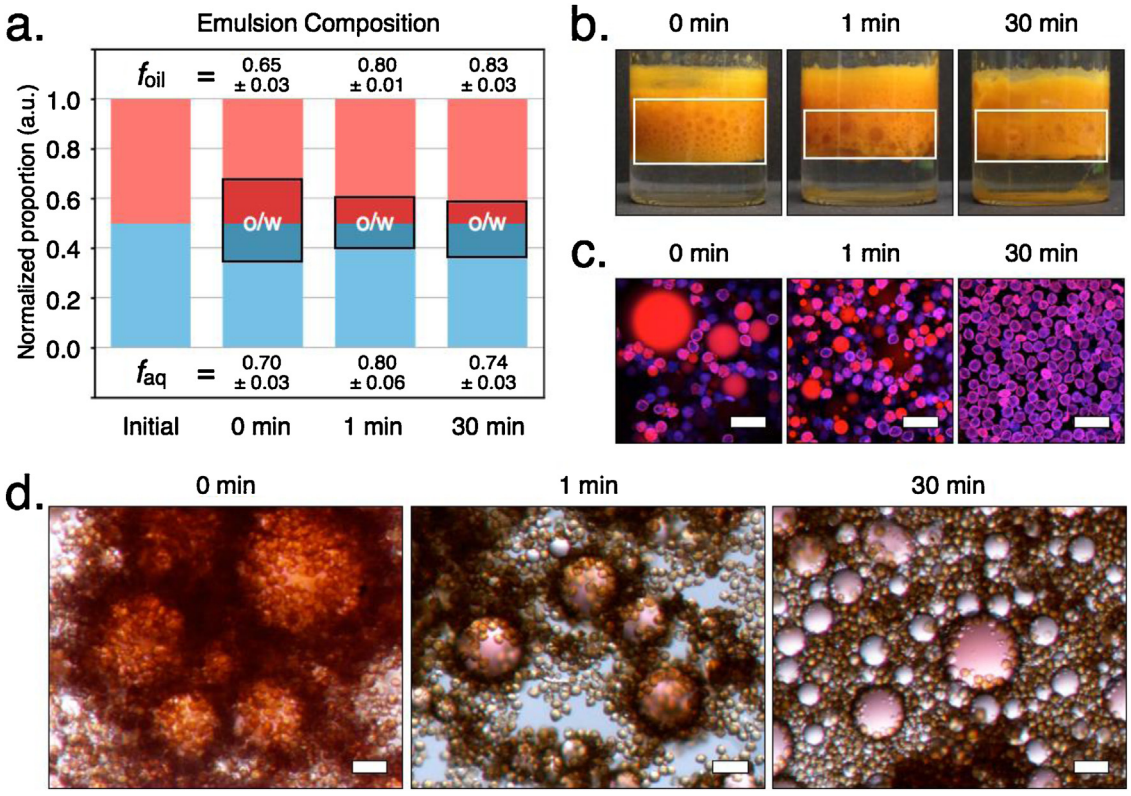

Fig. 4. Influence of ultraviolet-ozone (UV-O) treatment on oil/water emulsification properties of sporopollenin sporoderm microcapsules (S-SMCs). (a) Visual depictions of Pickering emulsion oil/water distributions. (b) photographs of representative Pickering emulsions. (c) CLSM images highlighting oil droplet and particle settling of Pickering emulsions with oil stained by Nile Red. Scale bars, 100 μm. (d) Stereomicroscopy images of Pickering emulsions incorporating the hydrophobic dye, Nile Red. Scale bars, 100 μm (For interpretation of the references to colour in this figure legend, the reader is referred to the web version of this article).

wall (Fig. 5a and Supplementary Information, Fig. S10). Upon further analysis of the loading distributions of oil-loaded S-SMCs for untreated and 30 min UV-O treated S-SMCs, it was observed that S-SMCs at the oil/water interface were only partially loaded for the untreated S-SMCs, and almost fully loaded for the 30 min UV-O treated S-SMCs. Isolation and quantification of the oil-loaded S-SMCs indicated that 0 min and 30 min UV-O treatment resulted in fully loaded particle proportions of 26.5 ± 5.4 % and 93.2 ± 3.7 %, respectively (Fig. 5b and Supplementary Information, Fig. S10).

It is proposed that the untreated S-SMCs have a greater affinity to the external oil in the oil/water system, and therefore any of the fully-, partially-, or un-loaded S-SMCs may be drawn up with the oil as the oil rises during system stabilization (Fig. 5c). However, 30 min UV-O treated S-SMCs become superhydrophilic and have minimal affinity to the oil in the oil/water system, and therefore only the fully-loaded particles rise due to the buoyancy of the internally encapsulated oil, whereas the partially- or un-loaded S-SMCs settle to the bottom of the oil/water system. Based on average values from S-SMC morphological and density analysis above, and the density of cocoa butter (0.976 g cm^{-3}) used in this study, the force of buoyancy (F_b) versus the force of gravity (F_g) for volumetric oil-loading of oil-loaded S-SMCs in water indicates that at 90 % loading $F_b < F_g$ (166.8 pN vs 167.0 pN), 95 % loading $F_b = F_g$ (174.0 pN vs 174.0 pN), and 100 % loading $F_b > F_g$ (181.3 pN vs 181.0 pN). The results indicate that at 95 % volumetric loading of cocoa butter ($F_g = F_b$) there will be a transition from sinking oil-loaded S-SMCs to floating oil-loaded S-SMCs, which is in strong agreement with the experimental observations.

Upon evaporation of the water containing the oil-loaded S-SMCs, it is possible to obtain a dry microparticle system with a high-degree of oil loading and minimal residual oil on the S-SMCs surface (Fig. 5d and Supplementary Information, Fig. S11). Importantly, it is proposed that with further optimization such a system may be automated to recycle the partially- or un-loaded S-SMCs so as to achieve an industrially scalable process for obtaining an efficient and continuous supply of fully oil-loaded S-SMCs.

3.5. UV-O exposure alters particle/cell interactions

Particle/cell interactions are different between untreated and UV-O treated S-SMCs with pronounced differences in both S-SMC particle distributions and cell proliferation distributions (Fig. 3d and Supplementary Information, Fig. S5b). Overall, with 24 h incubation on a stable layer of Huh-7.5 liver hepatocytes, total S-SMC particle binding proportions were similar for both untreated and UV-O treated S-SMCs, resulting in 84.5 ± 3.6 % and 75.2 ± 5.5 % of particles being bound by cells, respectively. The data indicates that cells will bind well with both untreated and UV-O treated S-SMCs. However, for untreated S-SMCs, particles tend to form clusters on the scale of 100–400 μm, and the cells proliferate both throughout the S-SMC clusters and uniformly across the polystyrene dish surface. Whereas for UV-O treated S-SMCs, particles disperse more uniformly tending to form single or double layers, and cell proliferation is focused over the UV-O treated S-SMCs with notably reduced spreading across the polystyrene dish surface.

Image processing of CLSM micrographs was conducted to quantify the coverage areas of S-SMCs and cells for both untreated and UV-O treated S-SMCs systems (Fig. 6a and Supplementary information, Fig. S13). S-SMC particle coverage increases with UV-O treatment from 37.3 ± 2.2%–60.7 ± 5.5 %, whereas cell coverage decreased from 85.4 ± 6.0%–63.5 ± 4.9 % suggesting that the cell proliferation dynamics are different in systems with untreated and UV-O treated S-SMCs (Fig. 6b). The proportion of S-SMC/cell overlap also increases with UV-O treatment from 30.2 ± 5.5%–43.9 ± 6.2

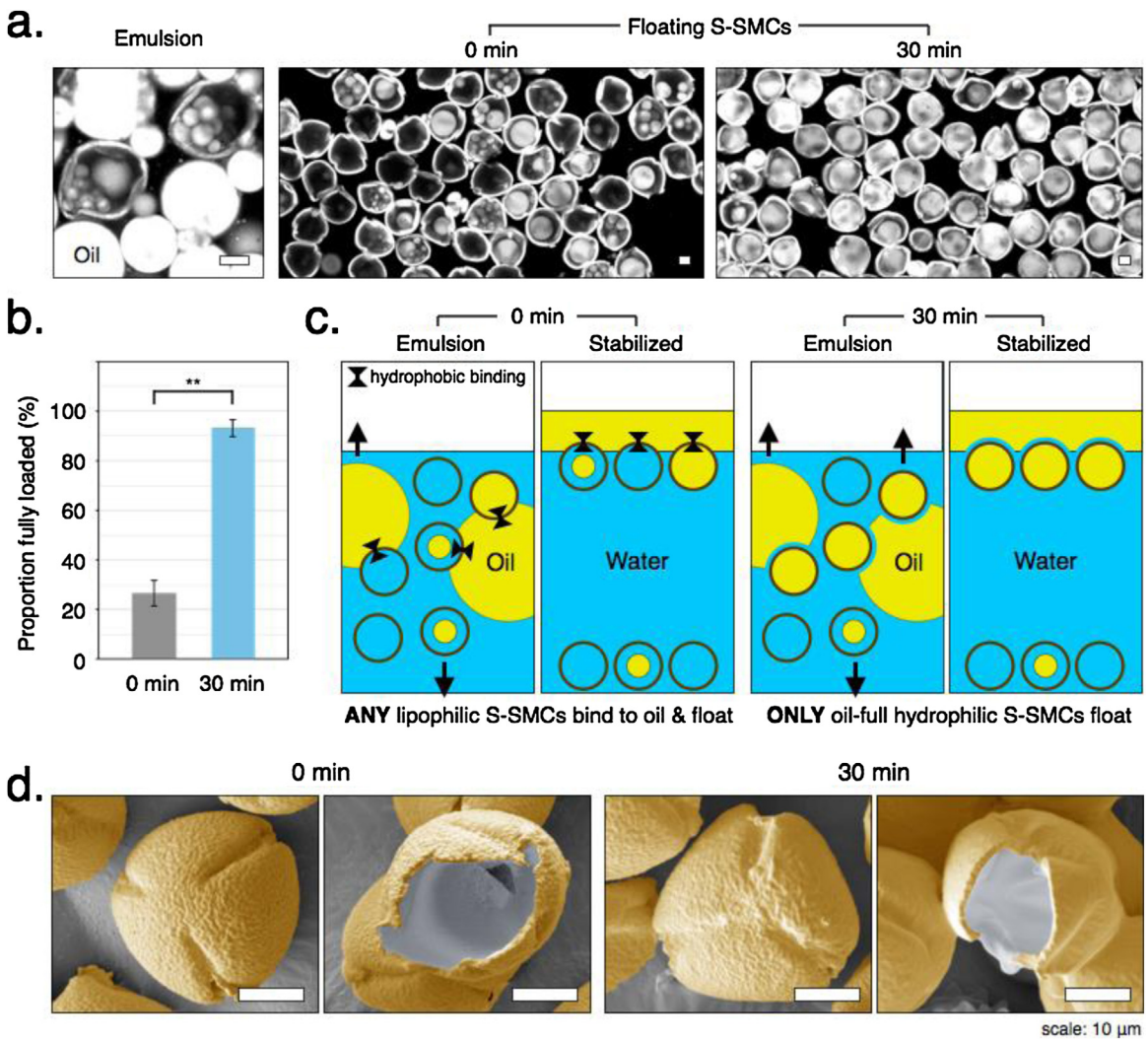

Fig. 5. Influence of ultraviolet-ozone (UV-O) treatment on oil loading of sporopollenin sporoderm microcapsules (S-SMCs). (a) CLSM cross-sectional images of an oil/water system with homogenization, and floating oil-loaded S-SMCs isolated after system stabilization. Scale bars, 10 μm. (b) Quantification of the proportion of fully oil-loaded floating S-SMCs. (c) Schematic representation of the proposed mechanisms of oil loading and system stabilization. (d) False-color SEM images of dried oil-loaded S-SMCs highlighting clean particle surface and representative oil loading (original uncolored images can be found in Supplementary Information, Fig. S11). Scale bars, 10 μm.

%, but may be attributed to the increase in total S-SMC coverage in the UV-O treated system. Most importantly, the proportion of non-S-SMC area covered by cells significantly ($p < 0.01$) decreases with UV-O treatment, with 88.0 ± 7.7 % of the untreated system non-S-SMC area covered by cells, yet only 50.2 ± 3.9 % of the UV-O treated system non-S-SMC area is covered by cells. Overall, these results indicate that cells tend to proliferate more around the UV-O treated S-SMCs. UV-O treatment altering substrate/cell binding dynamics is consistent with previous observations with defatted pollen and other synthetic polymers [25,54–56].

Observation of particle/cell spheroids and networks by CLSM and SEM provides further insights into particle/cell dynamics (Fig. 6c and Supplementary Information, Fig. S15). For untreated S-SMC systems, particle/cell spheroidal structures are observed along with cells proliferating throughout the 3D S-SMC system, and a thick layer of cells is visible covering the surrounding polystyrene dish. For UV-O treated S-SMC systems, particle/cell network structures are observed along with cells proliferating throughout the S-SMC network, and beyond a distance of ~20 μm from the S-SMCs there are large clear regions of polystyrene dish with no cell coverage. Close-ups of both systems indicate that cells are behaving like a mortar by binding the discrete S-SMCs together. During the washing of samples for extraction of non-bound S-SMCs, it was observed that both the particle/cell spheroid structures and single layer particle/cell network structures are robust and resistant to dissolution with agitation of the system (Supplementary Information, Movie S1).

Based on these observations, both untreated S-SMCs and UV-O treated S-SMCs provide compelling materials for use in cellular adhesion and tissue engineering applications. Through protocol variations and longer duration studies it may be possible to provide important contributions for developing novel spheroidal or network-type cell culture platforms [57]. Additionally, both untreated and UV-O treated S-SMCs exhibit the potential for cell compatibility and may be used for developing novel applied systems for oral, intravenous, or topical drug delivery.

4. Conclusions

UV-O treatment enhances the utility of acid-extracted S-SMC hollow microcapsules for colloidal, microencapsulation, and tissue engineering applications. Highly versatile S-SMCs may be extracted from bee-collected pollens and surface functionalized with short duration exposure to UV-O resulting in wetting properties rang-

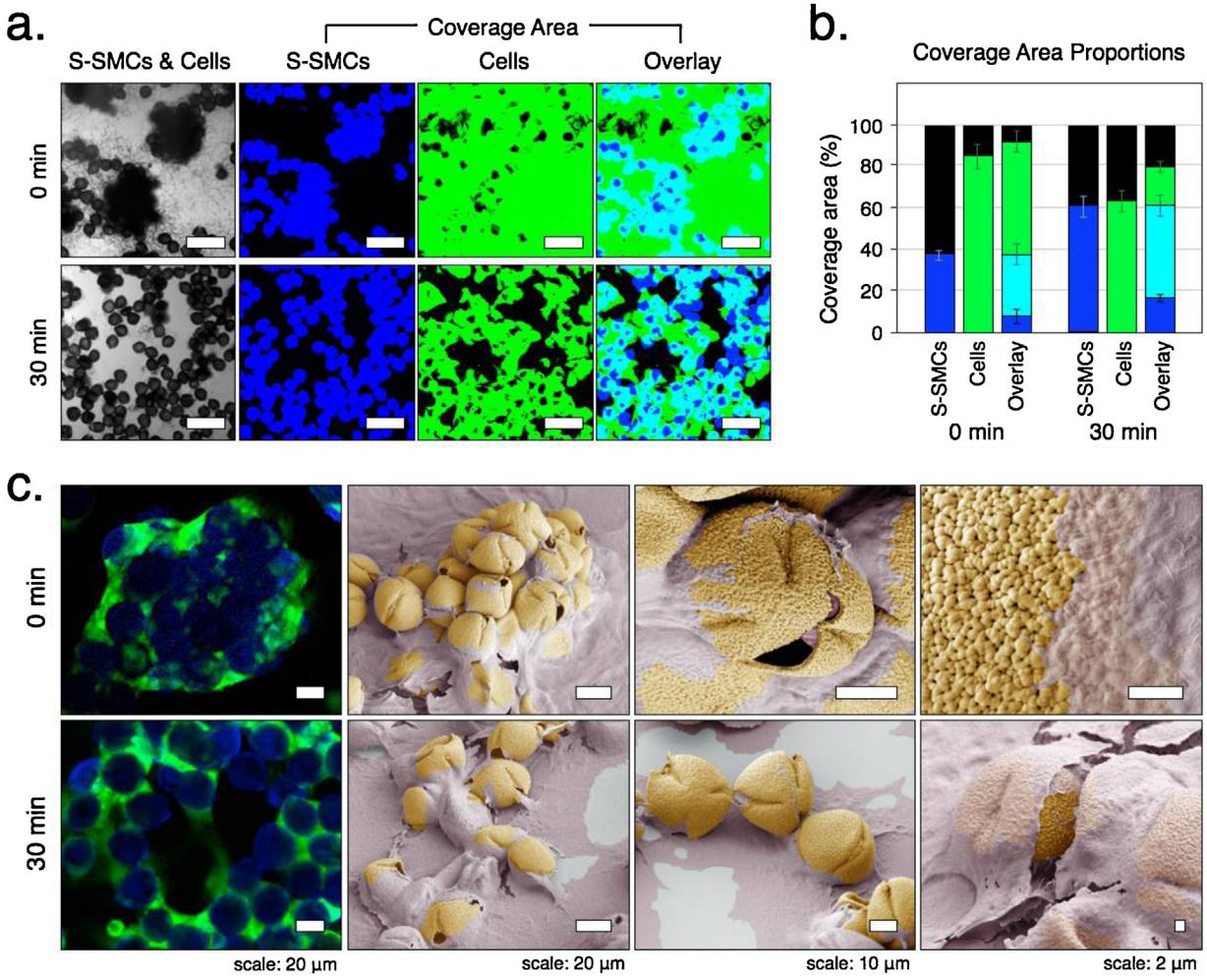

Fig. 6. Influence of ultraviolet-ozone (UV-O) treatment on sporopollenin sporoderm microcapsule (S-SMC)/cell interactions with Huh-7.5 liver hepatocytes. (a) CLSM images of S-SMC and cell distributions and coverage areas. Scale bars, 100 µm. (b) Quantification of S-SMC and cell coverage area proportions. (c) CLSM and false-color SEM images of representative S-SMC/cell spheroid and network structures (original uncolored images can be found in Supplementary Information Fig. S16).

ing from hydrophobic to superhydrophilic. The lipidic/aromatic copolymer exhibits oxidative alterations in surface chemistry by the chemisorption of atomic oxygen through the formation of ketone ($R_2C{=}O$) and ether (COC) bonds in conjunction with the ring opening and alteration of aromatic moieties within the copolymer structure. Both ketone and ether functionalities are considered hydrophilic and may be directly attributed to the observed enhancement in wetting and hydrophilic properties of the co-polymer structure. Modification of the surface chemistry of the acid-extracted S-SMCs provides an important means to tune the interfacial properties of the material for achieving desirable behaviors in various fundamental systems and applications.

Understanding the influence of surface modification on the behavior of S-SMCs in various applications provides insights into how the UV-O treatment of S-SMCs may be utilized to control systems of interest. In oil/water systems, untreated and short duration (1 min) UV-O treated S-SMCs are shown to form microparticle stabilized Pickering emulsions. However, beyond 1 min UV-O treatment, superhydrophilic S-SMCs fail to form a stable emulsion, yet lead to a means to obtain ideal fully oil-loaded microparticles. Both untreated and UV-O treated S-SMCs are shown to exhibit favorable particle/cell interaction dynamics, with untreated S-SMCs offering a means to obtain a novel particle/cell spheroid system, and UV-O treated S-SMCs resulting a more disperse particle/cell network system with increased particle/cell interaction.

Overall, S-SMCs and UV-O surface functionalization are shown to provide a highly versatile technology for utilization in a wide range of potential applications and there is much potential for the further exploration of the systems highlighted in this study. The behavior of UV-O treatment on S-SMC stabilized Pickering emulsion properties with various oil phase compounds, a detailed analysis of oil-loading of S-SMCs for various microencapsulation applications, and the optimization of particle/cell spheroids or 3D network structures for various tissue engineering applications all warrant further investigation.

Author contributions

E.L.T, M.G.P., G.F., J.A.J., and N.J.C. conceived and designed the experiments. E.L.T, M.G.P., G.F., and L.W. performed all the experiements. The manuscript was written by E.L.T, M.G.P., and J.A.J. All authors discussed the results and reviewed the manuscript.

Data availability

The data that support the findings of this study are available from the corresponding authors on request.

Acknowledgements

The authors acknowledge technical support from Ms. Ekaterina Stonkevitch. This research was supported by the Creative Materials Discovery Program through the National Research Foundation of Korea (NRF) funded by the Ministry of Science, ICT, and Future Planning (NRF- 2016M3D1A1024098). This work was also supported by the Competitive Research Programme (NRF-CRP10-2012-07) of the National Research Foundation of Singapore (NRF). The research was also supported by a Start-Up Grant (SUG) from Nanyang Technological University (M4080751.070). Many thanks are due to Dr. Y. N. Liang from the Nanyang Environment & Water Research Institute (NEWRI) for collection of the XPS data and to Dr. S. Pedersen for assistance with utilizing R-Code for data analysis.

Appendix A. Supplementary data

Supplementary material related to this article can be found, in the online version, at doi:https://doi.org/10.1016/j.apmt.2019.100525.

References

[1] S. Barrier, et al., Green Chem. 12 (2010) 234–240.
[2] C. Chiappe, et al., Green Chem. 19 (2017) 1028–1033.
[3] S.P. de Souza, et al., Catal. Sci. Technol. 5 (2015) 3130–3136.
[4] R.C. Mundargi, et al., Small 12 (2016) 1167–1173.
[5] M.G. Potroz, et al., J. Vis. Exp. (2016), e54768-e54768.
[6] I. Sargin, et al., Int. J. Biol. Macromol. 105 (2017) 749–756.
[7] W.B. Goodwin, et al.,Bioinspir. Biomim. 12 (2017), 066009.
[8] O.O. Fadiran, J.C. Meredith, J. Mater. Chem. A Mater. Energy Sustain. 2 (2014) 17031–17040.
[9] I.J. Gomez, et al., J. Mater. Chem. C Mater. Opt. Electron. Devices 3 (2015) 632–643.
[10] L. Wang, et al., Nano Energy 36 (2017) 38–45.
[11] H. Wang, et al., Adv. Funct. Mater. 27 (2017).
[12] L. Wang, et al., Adv. Funct. Mater. 26 (2016) 8623–8630.
[13] T. Baran, et al., J. Colloid Interface Sci. 486 (2017) 194–203.
[14] N.F. Ahmad, et al., Environ. Sci. Pollut. Res. Int. 24 (2017) 21846–21858.
[15] G. Mackenzie, et al., Front. Mater. Sci. 2 (2015) 66.
[16] W. Montgomery, et al., Macromol. Chem. Phys. 217 (2016) 2494–2500.
[17] A. Wakil, et al., Lipids 45 (2010) 645–649.
[18] M. Lorch, et al., Chem. Commun. (Camb.) 42 (2009) 6442–6444.
[19] B.P. Binks, et al., Soft Matter 7 (2011) 4017–4024.
[20] Y. Sakurai, et al., Colloid Polym. Sci. 295 (2017) 413–420.
[21] O. Naas, et al., Environ. Pollut. 214 (2016) 816–821.
[22] P.F. van Bergen, et al., Evol. Plant Physiol. (2004) 133–145.
[23] M.J. Walzak, et al., J. Adhes. Sci. Technol. 9 (1995) 1229–1248.
[24] A.M. Amat, et al., Appl. Catal. B 23 (1999) 205–214.
[25] E.L. Tan, et al., Adv. Funct. Mater. 28 (2018).
[26] P.E. Jardine, et al., J. Micropalaeontol. 34 (2015) 139–149.
[27] C. Jungfermann, et al., J. Plant Physiol. 151 (1997) 513–519.
[28] H. Lin, et al., J. Colloid Interface Sci. 442 (2015) 133–139.
[29] L.R. Johnstone, et al., ACS Appl. Mater. Interfaces 9 (2017) 24804–24811.
[30] B.P. Binks, et al., Langmuir 21 (2015) 8161–8167.
[31] S. Noppakundilograt, et al., Carbohydr. Polym. 131 (2015) 23–33.
[32] W.J. Lee, et al., J. Food Eng. 222 (2018) 100–109.
[33] S. Barrier, et al., J. Mater. Chem. 21 (2011) 975–981.
[34] A. Diego-Taboada, et al., J. Mater. Chem. 22 (2012) 9767–9773.
[35] S.U. Atwe, et al., J. Control. Release 194 (2014) 45–52.
[36] M.J. Uddin, H.S. Gill, J. Control. Release 268 (2017) 416–426.
[37] M.W. Laschke, M.D. Menger, Trends Biotechnol. 35 (2017) 133–144.
[38] M. Gionet-Gonzales, K. Leach,Biomed. Mater. 13 (2018), 034109.
[39] K. Uto, et al., Prog. Polym. Sci. 65 (2017) 53–82.
[40] C. Wang, et al., ACS Appl. Mater. Interfaces 7 (2015) 17545–17551.
[41] R.C. Mundargi, et al., Sci. Rep. 6 (2016) 19960.
[42] A.K. Prabhakar, et al., J. Ind. Eng. Chem. 53 (2017) 375–385.
[43] M.G. Potroz, et al.,Adv. Funct. Mater. 27 (2017), 1700270.
[44] M.K. Corliss, et al., J. Ind. Eng. Chem. 61 (2017) 255–264.
[45] B. Gurzęda, et al., RSC Adv. 7 (2017) 19904–19911.
[46] H.J.B. Birks, et al., Science 354 (2016) 412–413.
[47] J.-L. Li, et al.,Phys. Rev. Lett. 96 (2006), 176101.
[48] R. Larciprete, et al., J. Phys. Chem. C 116 (2012) 9900–9908.
[49] M. Bağcıoğlu, et al.,PLoS One 10 (2015), e0137899.
[50] P.E. Jardine, et al., Rev. Palaeobot. Palynol. 238 (2017) 1–6.
[51] M.D. Romero-Sánchez, et al., Int. J. Adhes. Adhes. 25 (2005) 358–370.
[52] M. Sapiña, et al., J. Chem. Technol. Biotechnol. 92 (2017) 210–216.
[53] J. Peeling, D.T. Clark, J. Polym. Sci. Part A: Polym. Chem. 21 (1983) 2047–2055.
[54] D. Teare, et al., Langmuir 16 (2000) 2818–2824.
[55] K. Kasai, et al., Mater. Sci. Eng. C 78 (2017) 354–361.
[56] K. Saha, et al., Proc. Natl. Acad. Sci. U.S.A. 108 (2011) 18714–18719.
[57] D. Hetemi, J. Pinson, Chem. Soc. Rev. 46 (2017) 5701–5713.